



AMERICAN JOURNAL OF  
**CHEMISTRY AND PHARMACY (AJCP)**

ISSN: 2834-0116 (ONLINE)

**VOLUME 2 ISSUE 2 (2023)**

PUBLISHED BY  
**E-PALLI PUBLISHERS, DELAWARE, USA**

## A Review on the Utilization and Environmental Concerns of Coal Fly Ash

Saidu Kamara<sup>1</sup>, Edward Hingha Foday Jr<sup>2</sup>, Wei Wang<sup>1\*</sup>

### Article Information

**Received:** April 26, 2023**Accepted:** June 10, 2023**Published:** July 02, 2023

### Keywords

*Characterization, Silica, Coal, Combustion, Fly Ash*

### ABSTRACT

Coal is a well-known source of electric power generation all over the globe. Pulverized coal combustion and fluidized coal bed combustion are the two conventional methods involved in the combustion of coal in thermal power plants. Pulverized coal combustion is operated at >1400°C while the fluid bed is operated at a temperature between 850-900°C. The first two reactions are the main reactions in the coal combustion process and they are exothermic reactions. CO<sub>2</sub> and CO are the first two combustion products. The inorganic minerals in coal are released as waste products in the combustion plants in which fly ash made a large part of the waste materials. Fly ash is formed due to the incomplete combustion of coal. The fly ash from both methods contains SiO<sub>2</sub>, Al, etc, which are significant constituents. High-grade coal has a higher SiO<sub>2</sub> than the low grade. An experiment was conducted by preparing four samples of fly ash heated at 500°C, 600°C, 700°C, and 800°C, and one unheated sample to investigate the chemical composition of the fly ash obtained from Xi'an Linyuan Silica Limited and to prove its suitability as raw material for the fabrication of refractory composites. SEM, EDS, XRD, and FTIR characterization were done on all five samples to determine the chemical parameters of the fly ash. According to the result and analysis of the four characterizations, it was discovered that the fly ash used in this research contains SiO<sub>2</sub>. SEM/EDS morphological analysis reveals the presence of spherical and a few geometrical crystalline-shaped structures known as cenospheres. Cenospheres are important components for the synthesis of refractory composites. The EDS micrographs show the percentages of silicon and oxygen in the fly ash. The FTIR results show Si-O-Si stretching in all the fly ash prepared samples. In the XRD, it was discovered that the fly ash was purely SiO<sub>2</sub>.

### INTRODUCTION

The popular source of electric power generation around the world today is coal utilized in pulverized coal combustion and fluid bed combustible conventional plants (S. H. Lee, Lee, Jeong, & Lee, 2019; Miller, 2010). The two different combustion methods operate at different temperatures and therefore each method produces different fly ash with different characteristics (Erol, Küçükbayrak, & Ersoy-Mericboyu, 2008; L. Li, Wang, & Zhu, 2006; Molina & Poole, 2004). The temperature range in the coal fluid bed is 8500C-9000C while the temperature in pulverized combustion is between 14000C-15000C. At temperatures greater than 14000C (>14000C), minerals such as the aluminosilicate present in coal disintegrate or decompose (Mishra & Baliarsingh, 2008; Pavlish *et al.*, 2003; Rios Reyes, 2008). The disintegrated mineral particles form hollow or spherical objects called cenospheres as a result of rapid cooling that takes place during the post-combustion phase (Kim, 2002; Pundienė, Korjakins, Pranckevičienė, & Kligys, 2018). High melting point minerals sometimes remain unaltered. The physical and chemical composition of fly ash is significantly influenced by the type of coal used and the variation in combustion temperatures (Adriano, Page, Elsewi, Chang, & Straughan, 1980; Pedersen, Jensen, Skjøth-Rasmussen, & Dam-Johansen, 2008; Ratafia-Brown, 1994). Both two types of combustion processes contain Al, SiO<sub>2</sub>, Fe, and Ca which are the four most constituents in fly ash (Cheng

& Chen, 2003; Criado, Fernández-Jiménez, De La Torre, Aranda, & Palomo, 2007). The fly ash produced from coal fluidized beds (CBD) has no mullite and glass balls. It contains high quantities of unburnt carbon, calcium carbonate, and calcium sulfate and it forms irregular objects. Unburned carbon exists in both types of fly ash (Batra, Urbonaite, & Svensson, 2008; Maroto-Valer, Taulbee, & Hower, 2001). Fly ash is among the popular global raw material and one of its most important utilization is in the fabrication of composites (Gollakota, Volli, & Shu, 2019). In addition to the current global use of fly ash, further research and development are required to enhance the management of fly ash and bring out new techniques to control the end products that result from burning coal.

Harmful elements and compounds such as aromatic compounds, carbon, silica, fine particulate matter, etc., are aggregated in high concentrations during combustion (Schwarze *et al.*, 2006; Valavanidis, Fiotakis, & Vlachogianni, 2008). Thermal power plants produce enormous inorganic particles and emit combustible gases into the atmosphere which negatively affects the health of residents around the thermal plants (Rahman, Farrok, & Haque, 2022). The thermal industries have no use for the ash generated and therefore regard it as a solid waste product with the potential to negatively impact the environment if not properly regulated (Foday Jr *et al.*, 2017). A small amount (~20%) of the global fly ash

<sup>1</sup> Department of Chemical Engineering, School of Water and Environment, Chang'an University, Xi'an, China

<sup>2</sup> Key Laboratory of Subsurface Hydrology and Ecology in Arid Areas, Ministry of Education, Chang'an University, Xi'an, China

\* Corresponding author's e-mail: [ksaidu2013@gmail.com](mailto:ksaidu2013@gmail.com)

produced annually, is used for many purposes and the rest reportedly contributes to the existing global pollution trend.

Characterizations using SEM, EDS, XRD, FTIR, etc, to determine the composition of fly ash have been studied. Several past works on the two types of fly ash were centered on their properties, morphology, and chemical composition. In this study, the morphology and chemical information of the fly ash samples is determined by SEM and EDS. The XRD reveals information about the crystalline size and amorphous phase of the samples. The in-situ functional groups (Si-O-Si, C-O, Al-O, etc,) in fly ash are accounted for by the Fourier transform infrared spectroscopy (FTIR). These functional groups are the typical determinants for the use of fly ash as raw material for the synthesis of composites. This experiment, therefore, studies the characterization of purified fly ash from the Xi'an Linyuan silica limited.

The major problem encountered in the characterization of fly ash is the amorphous phase of the sample which is normally not captured by the XRD. A more adequate instrument is therefore required for the characterization of fly ash to identify its glass phase and interpret chemical composition. EDS is the most common effective tool used for this purpose but the contrasting characteristics of fly ash present a large scattered result that makes the analysis very difficult. In recent times, new EDS technology or detectors have been invented with the capability to collect the spectrums of all pixels in not more than an hour. The spectra collected are further processed into maps that show the elemental intensities used to quantify the chemical compositions of the elements present.

## LITERATURE REVIEW

### Process and end products of coal combustion

Coal constitutes inorganic minerals released as waste products (fly ash, bottom ash, and slag) during the burning of coal. The greater part of the waste products in the combustion plant is made of fly ash. Fly ash is made of fine light particles and has a density of about  $2.5\text{g/cm}^3$  bottom ash is composed of coarse particles while slag is the melted phase of bottom ash (Bourtsalas, 2015; Bunge, 2015). The ash generated in the combustion plant is made of a large mass of oxides (silica, alumina, titanium oxide, magnesium oxide, calcium oxide, sulfoxide, etc,) and heavy metals (zinc, lead, copper, nickel, cobalt, cadmium, etc,)(Foday Jr, Bo, & Xu, 2021; Halmann, 1995; Oves, Khan, Zaidi, & Ahmad, 2012). Fly ash contains some quantities of spherical matter called cenospheres formed by the decomposed minerals in the condensation or cooling stage (Blissett & Rowson, 2012; Fenelonov, Mel'gunov, & Parmon, 2010; Oves *et al.*, 2012; Vassilev, Baxter, Andersen, & Vassileva, 2013).

Fly ash is formed due to the incomplete combustion of the mineral components in coal which subsequently transform into some crystalline phases called quartz (silica), magnetite, aluminosilicate glass (mullite), spinel, etc. It is confirmed that fly ash is made of over 80% of silica ( $\text{SiO}_2$ )(Criado *et al.*, 2007; Joshi & Lohita, 1997; Vassilev & Vassileva, 1996). The glass phase in fly ash is formed from low-grade bituminous coals which constitute lesser quantities of silica and a higher amount of magnetite compared to high-grade bituminous coal which composes high silica content. The process leading to the formation of fly ash is explained in figure 1 below:

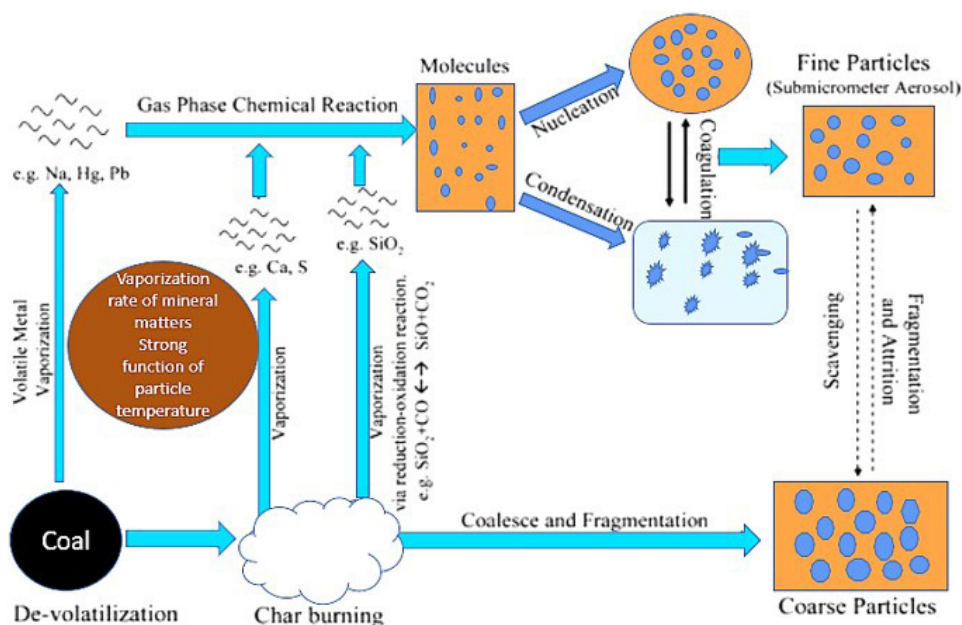
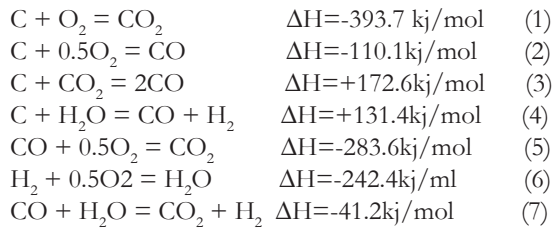


**Figure 1:** A modified schematic diagram for the formation of fly ash

The process begins with vaporizable components which nucleate to produce new crystalline objects, form char and release heavy metals by vaporization.

### Reactions in coal combustion

The carbon in coal undergoes the following chemical reaction with oxygen.



The reaction is exothermic when the enthalpy  $\Delta H$  change is negative (i.e. heat is given out during the reaction) while a positive enthalpy  $\Delta H$  means the reaction is endothermic (i.e. heat is absorbed during the reaction). The first two reactions are the main combustion reactions according to their products.  $\text{CO}_2$  and  $\text{CO}$  are the first combustion products and their ratios increase with an increase in temperature and a decrease in pressure. The whole combustion process leading to the formation of a coal boiler takes about two seconds.

### Mathematical models for fly ash deposition in a boiler tube

Mathematical models are employed to determine the activity of ash precipitation and to ameliorate the lapses in industrial design (Fan, Zha, Sun, & Cen, 2001). The prediction of ash deposition has been done by a good number of researchers using experimental notations but it becomes misleading when taking into consideration other operating factors (Fan *et al.*, 2001; Zeng, Zheng, Zhou, Fang, & Lou, 2016). The deposition of ash in boilers has been adequately studied with the application of numerical procedures. Fly ash data obtained from a computer control scanning electron microscope has been used to develop a fly ash prediction model (F. Lee & Lockwood, 1999). The temperature, porosity, and rate of deposition were simulated by Galen *et al.* (Richards, Slater, & Harb, 1993).

### Particle Movement Expressions

Newton's equation of motion below is used to account for the particle movement in a pulverized boiler.

$$m_i \frac{dv_i}{dt} = m_i g + F_d + F_{th} \quad (8)$$

The drag force  $F_d$  is given by

$$F_d = -3\pi d\mu(v-u)f$$

where  $\mu g$  is the gas viscosity and  $f$  is the drag force coefficient that is used to revise the Stokes expression and assuming that  $f=1$ .

Waldmann equation below is used to determine the thermophoretic force (Waldmann & Schmitt, 1966)

$$F_{th} = -\frac{32}{15} \frac{K_{tr} r^2}{\bar{c}} \Delta T \quad (9)$$

Where

$K_{tr}$  is the thermal conductivity of the gas and  $\Delta T$  is the temperature gradient.

The mean speed  $\bar{c}$  of gas molecules is given by

$$\bar{c} = \sqrt{\frac{8k_B T}{\pi m_g}} \quad (10)$$

### Particle Collision Forces

The particle equation is used to compute the collision velocities of fly ash deposition in a boiler. To ensure efficient and smooth velocity collision, the particle in motion must be spherically rigid, the interaction forces and infinite forces should be impulsive and negligible respectively, and the particle movement should be centered and two-dimensional. The mathematical expression for a particle is given below (Hoomans, Kuipers, Briels, & van Swaaij, 1996).

$$m_i (v_{i,1} - v_{i,0}) = J \quad (11)$$

$$m_j (v_{j,1} - v_{j,0}) = -J \quad (12)$$

where,

$v_{i,0}$  and  $v_{i,1}$  is the pre-collisional and post-collisional velocities of particle  $i$ , and

$v_{j,0}$  and  $v_{j,1}$  are the pre-collisional and post-collisional velocities of particle  $j$ .

In the absence of particle-particle collision, we can also find the sample position using the single-particle equation at a time. The method of Monte Carlo is exclusively used to compute the particle-particle collision. If particle  $i$  collides with particle  $j$  in the time step, the post-collision velocities of particles are accounted for by taking into consideration the dynamics of the collisions. The velocities after particle collision will now substitute the initial particle velocities but the particles remain fixed in their fixed positions. The particle  $i$  in a time step  $\Delta t$  is determined by the probability of the collision below (Bird, 1994; Tsuji, Tanaka, & Yonemura, 1998):

$$P_i = \sum_{j=1}^N P_{ij} \quad (13)$$

$$P_{ij} = \frac{n}{N} \pi d^2 g_o v_{ij} \Delta t \quad (14)$$

where

$N$  is the number of simulated particles in the cell,

$n$  is the local particle number,

$d$  is the particle diameter,

$g_o$  is the radial distribution function,

$v_{ij}$  is the relative velocity between particle  $i$  and  $j$ , and

$\Delta t$  is the time step.

The collision pairs searching is the key problem in the calculation of particle-particle collision.

### Ash Deposition Model

During the process of ash deposition, the large ash particle causes an impact in the boiler tube and rebounds while the smaller ones can stick onto the tube with high adhesive energies (G. Li, Li, Huang, & Yao, 2015). The formation of the first layer improves the surface sticking capability in the tube. The critical velocity model is employed to ascertain if a particle motion sticks or rebounds in the boiler tube. The critical velocity equation is written as:

$$V_{critical} = \left( \frac{14.18}{m} \right)^{\frac{1}{2}} (W^5 R^4 / E)^{1/6} \quad (15)$$

Where,

$W$  is the adhesion energy and

$E$  is Young's modulus (S. Li, Marshall, Liu, & Yao, 2011; Liu, Li, & Yao, 2011).

According to the simulation of the critical velocity ( $V_{critical}$ ) expression above, the impact of the particle velocity is compared with the critical velocity. When the critical velocity of a particle is larger than the velocity impact, the particle clings to the surface.

## MATERIALS AND METHOD

Five samples of fly ash were measured on an electronic weighing scale. Each sample weighs 4g. Four of these samples were heated at 500°C, 600°C, 700°C, and 800°C for 3 hours in a muffle furnace and one remain unheated. The samples were then taken for SEM, EDS, XRD, and FTIR characterization. The aim was to determine the elemental characteristics of fly ash that make it a suitable raw material to synthesize refractory composites.

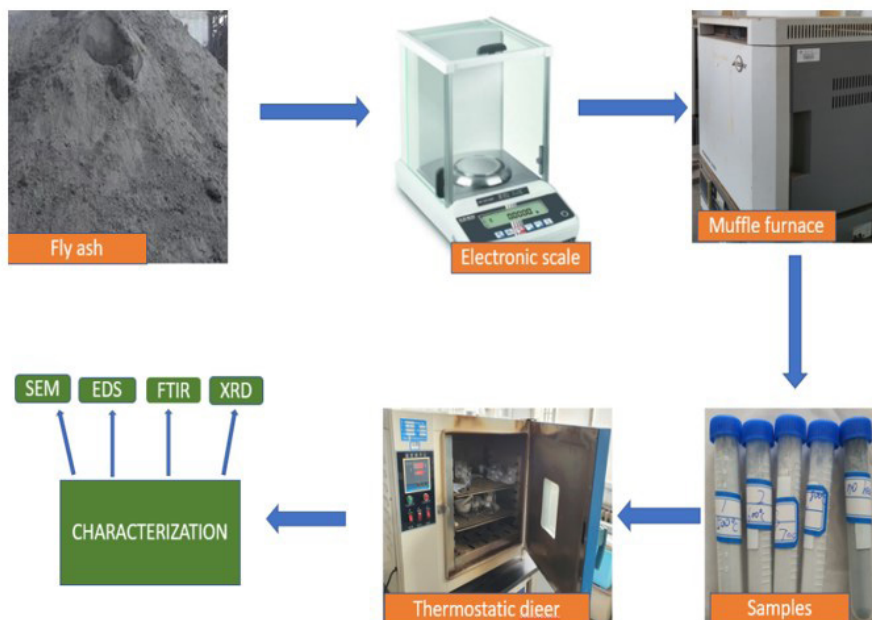


Figure 2: Illustration of instrumental setup and sample preparation

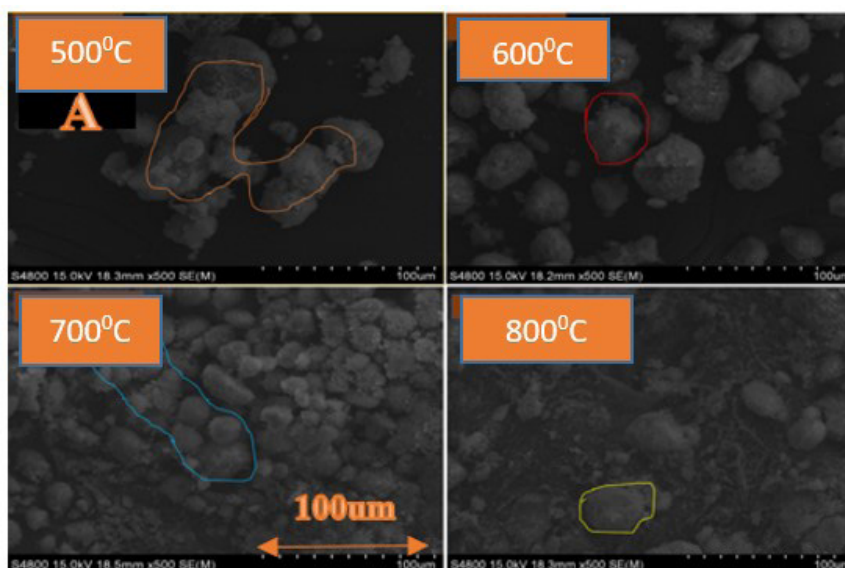
## RESULT AND DISCUSSION

### SEM Result

This technique is utilized by material scientists to determine and interpret the microstructure of materials. The sample electrons are bombarded to produce a wide range of emissions (such as X-rays, visible photons, auger electrons, secondary electrons, backscattered electrons, etc). The SEM result of the fly ash specimens is discussed as follows:

### Heated fly ash

Figures A and B below present the SEM results of four samples of fly ash heated at 5000C, 6000C, 7000C, and 8000C. The images in figure (A) above are the results of sample sizes scanned at 100 um pixels while figure B scanned image sizes at 20 um. The morphology of the images is based on the materials present in the fly ash samples.



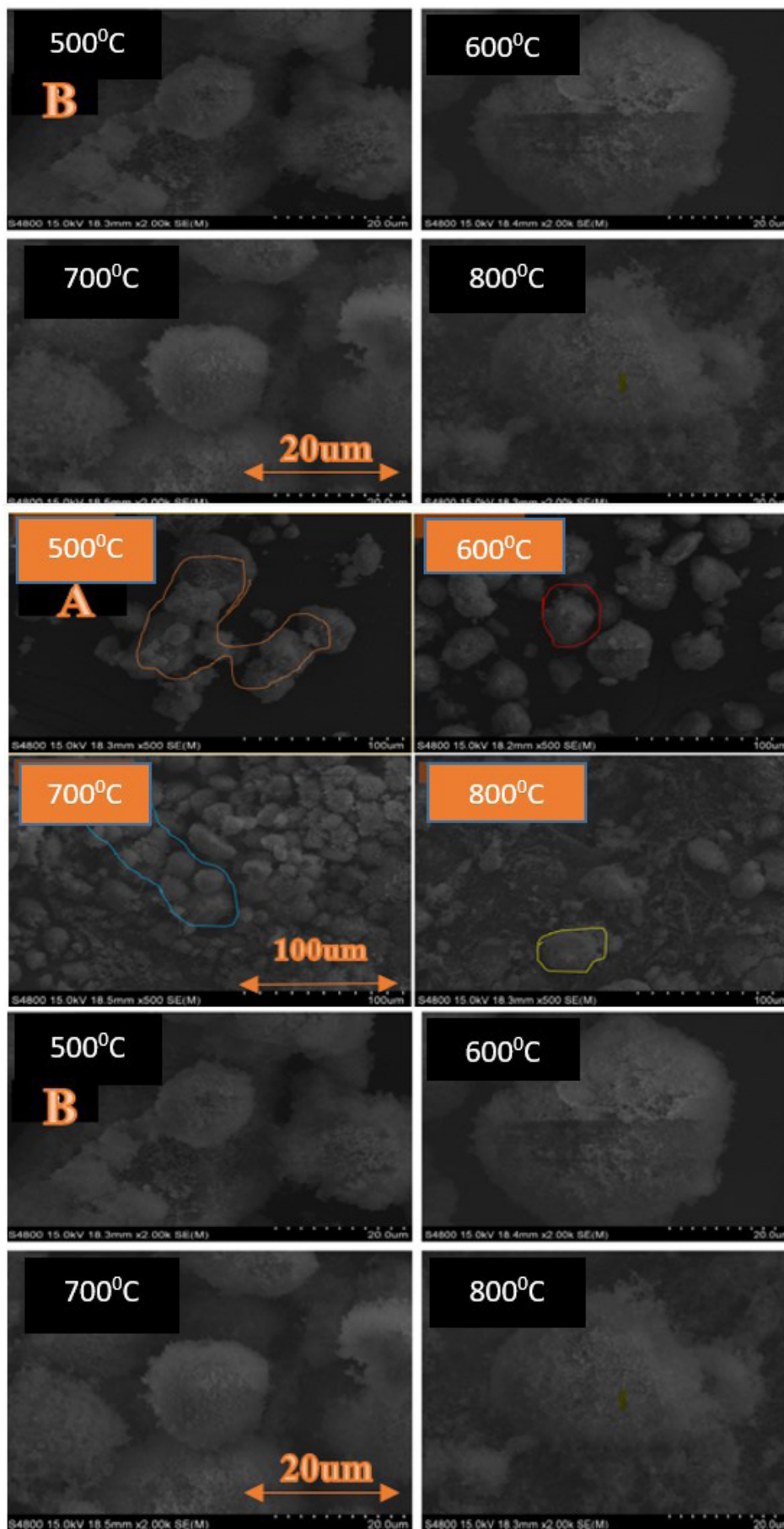


Figure 3: SEM images showing samples scanned at 100 μm in (A) and at 20 μm in (B).

All four sample images show un-interconnected irregular oval structured layers in both figures A and B. Few geometrically shaped structures are observed in sample 3. The agglomerated oval glassy and geometrically shaped structures are typical of the presence of silica crystalline structures in the sample materials. The balloon-shaped crystals are indicative of the presence of cenospheres in the fly ash samples. There are significant pore sizes in the samples and are observed to be highly visible in specimens 1, 2, and 4 but less in specimen 3. This shows that there might be other materials present in the samples but in less or insignificant quantities. All four samples heated at various temperatures show that quartz or silica is the dominant crystalline phase present in the fly ash sample. The samples were heated at temperatures that will lead to the elimination of carbon contents present in the fly ash with no chemical reaction taking place.



**Figure 4:** SEM images of unheated raw fly ash at three different magnifications

According to the micrographs, the oval crystalline structures become more pronounced as the temperature increases from 500°C, 600°C, 700°C, and 800°C. Conversely, the dark fields observed in the micrographs according to the morphology of the sample become lesser as the temperature is increased from sample one to four. This can be attributed to the carbon content which decreases as more temperature is applied to the fly ash.

### Unheated fly ash sample

Figure 4 shows the SEM micrographs of the unheated fly ash specimen with image sizes scanned at 200 um, 30 um, and 20 um pixels. The oval crystals are the same as those of the heated samples shown in figure 3 but are visibly observed to be far apart from each other compared to those seen in figure 3A above. This probably implies the presence of carbon content and other minor constituents that occupies the spaces between the crystals.

### EDS Result

This is a powerful analytical detector or tool used to determine the chemical elements present in a sample

and estimate their relative abundance. It relies on the interaction of some source of X-ray excitation and a sample. The capability of this tool is due to the fact or principle that each element has its unique structure that allows several peaks to display on its electromagnetic emission spectrum (which is the main principle of the electromagnetic spectrum).

In the emission of X-ray characteristics from a sample, a beam of electrons is focused on the sample under investigation. At rest, an atom within the sample contains ground state (or unexcited) electrons in discrete energy levels or electron shells bound to the nucleus. The incident beam may excite an electron in an inner shell, ejecting it from the shell and forming a hole in the initial position of the electron. An electron from an outer, higher-energy shell then fills the hole, and the difference in energy between the higher-energy shell and the lower-energy shell may be released in the form of an X-ray. The EDS is then used to measure the number and energy of the X-rays emitted from the sample. The detector or tool allows the elemental composition of the sample to be measured since the energies of the X-ray are characteristic of the atomic structure of the emitting element.

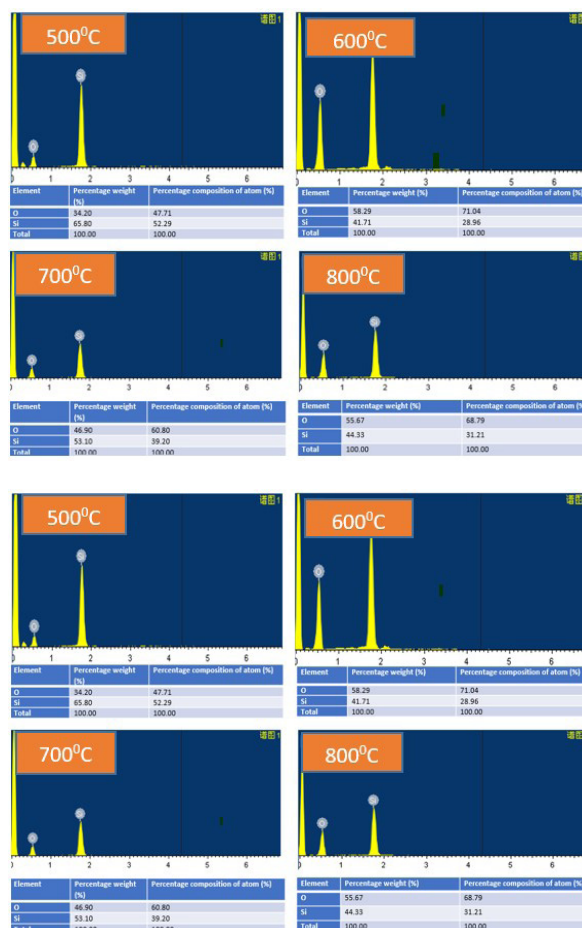


**Figure 5:** EDS result of heated fly ash specimens 1,2,3 & 4

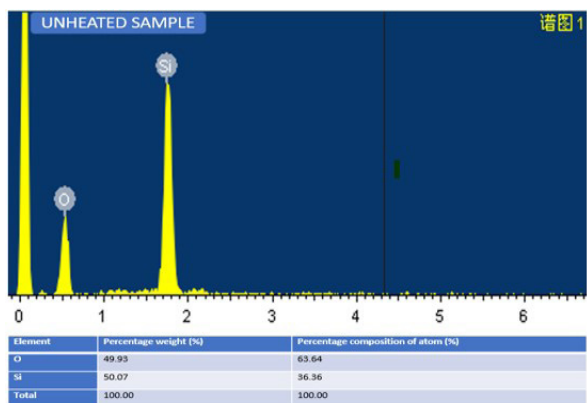


Figure 6: EDS result of unheated fly ash specimen

The EDS shown in figures 5 and 6 confirmed the percentage weight and elemental composition of both heated and unheated fly ash samples. According to the EDS result, oxygen and silicon are the predominating elements present in all five prepared samples. The percentage composition of oxygen is greater than that of silicon in all five samples. It is also observed from the elemental tables of the EDS figures that the weight percentage of silicon is higher in the first, third, and unheated samples than those of oxygen atoms but lesser in the second and fourth samples. The results and analysis

of this work show that fly ash used is silica pure and therefore a recommendable source for the fabrication of refractory composite materials.

### Cenospheres

According to the SEM and EDS results of this research, the hollow and spherical-shaped objects observed in all five samples depict the presence of cenospheres. Cenospheres are one of the end products in coal combustion and are significant components for the synthesis of refractory composites. They are formed as a result of the decomposition of the mineral matter in coal at high temperatures  $>1400^{\circ}\text{C}$ . The disintegrated or decomposed mineral matter form into spheres known as cenospheres during the post-combustion phase or cooling process. The decomposition of calcium carbonate and other compounds below  $1000^{\circ}\text{C}$  produces gases that blow up the minerals. The gases emitted during coal combustion inflate the decomposed minerals to form cenospheres. These objects are largely made of mullite, quartz (silica), aluminosilicate glass, calcite, sulfates, etc. Inside the balloon-shaped structure of the cenospheres are gases while the outer membrane or layer is made of aluminosilicate, cristobalite, quartz, mullite, etc. Cenospheres are discovered to be highly porous and can therefore effectively absorb water.

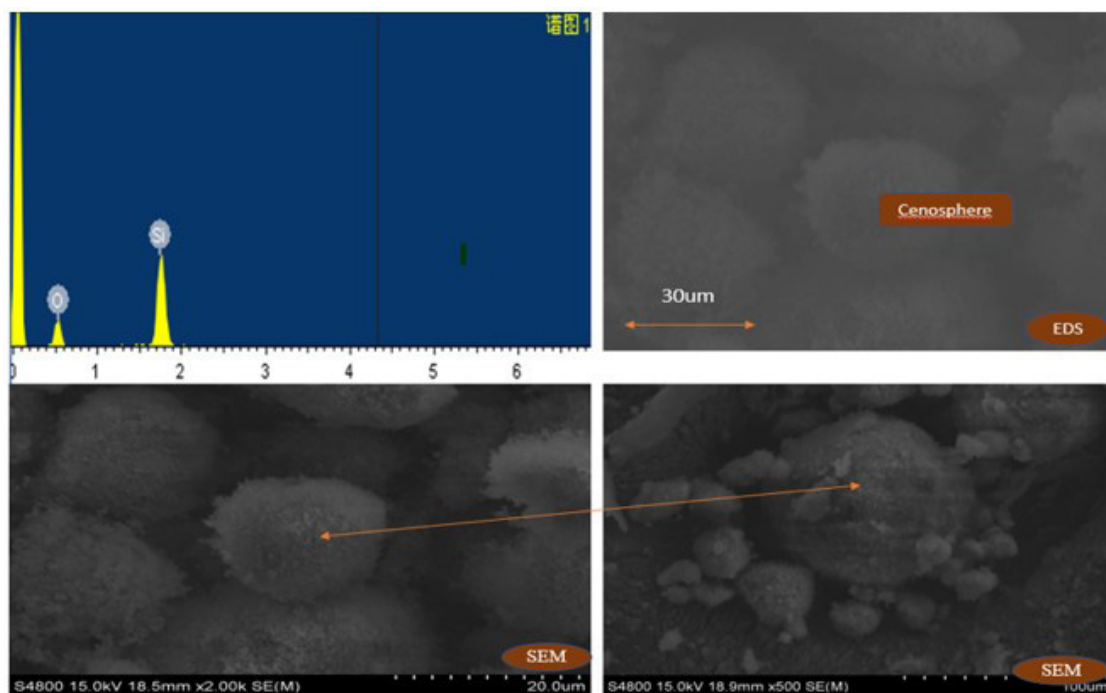


Figure 7: EDS and SEM micrographs showing cenospheres

The cenospheres discovered from the fly ash samples in this experimental research can be used for electronic and radar purposes due to their metallic and magnetic properties. Cenospheres are useful to refractory industrial engineers due to their low thermal conductivities and high heat resistance. They also have properties that are suitable to make lightweight composite materials used in aerospace engineering.

### FTIR Result

This technique is employed to study the vibrations of atoms in a molecule or compounds of a particular sample. The fractions of absorbed incident radiation at a particular energy are determined by passing Infrared (IR) radiation through the specimen. The FTIR results and analysis of the prepared fly ash specimens are discussed below.

### Heated Samples

The figure below shows the FTIR spectra obtained from the characterization of fly ash samples heated at 500°C, 600°C, 700°C, and 800°C. According to the experimental result of the sample heated at 500°C, a strong appearance of O=C=O bending of carbon dioxide compound is observed at a wavenumber of 2349cm<sup>-1</sup>. Further, the wavenumber 1083cm<sup>-1</sup> depicts the appearance of Si-O-Si stretching vibrations and strong absorption peaks while the 799cm<sup>-1</sup> wavenumber shows Si-O symmetric stretching of quartz.

Analysis of the FTIR experimental data for the sample heated at 600°C also depicts the appearance of O=C=O at 2349cm<sup>-1</sup> which indicates a strong vibrational stretching of the carbon dioxide compound. The wavenumbers

1090cm<sup>-1</sup> and 807cm<sup>-1</sup> indicate Si-O-Si and Si-O stretching vibrations respectively.

In sample three, the wavenumber 2363cm<sup>-1</sup> from FTIR results shows O=C=O bending but does not fall at 2349cm<sup>-1</sup> which is the strong absorption band for O=C=O. Therefore, the appearance of carbon dioxide compound at 2363cm<sup>-1</sup> can either be weak or medium. The frequency range for the absorption of O=C=O is 2400cm<sup>-1</sup>–2000cm<sup>-1</sup>. The wavenumber 1090cm<sup>-1</sup> and 803cm<sup>-1</sup> show the stretching vibrations of Si-O-Si and Si-O respectively. The FTIR of the fourth sample heated at 800°C shows the absorption frequencies of 2369cm<sup>-1</sup>, 1123-1027cm<sup>-1</sup>, and 798cm<sup>-1</sup>. The wavenumber 2369cm<sup>-1</sup> shows weak or medium O=C=O stretching vibrations while 798cm<sup>-1</sup> depicts the Si-O symmetric of quarts.

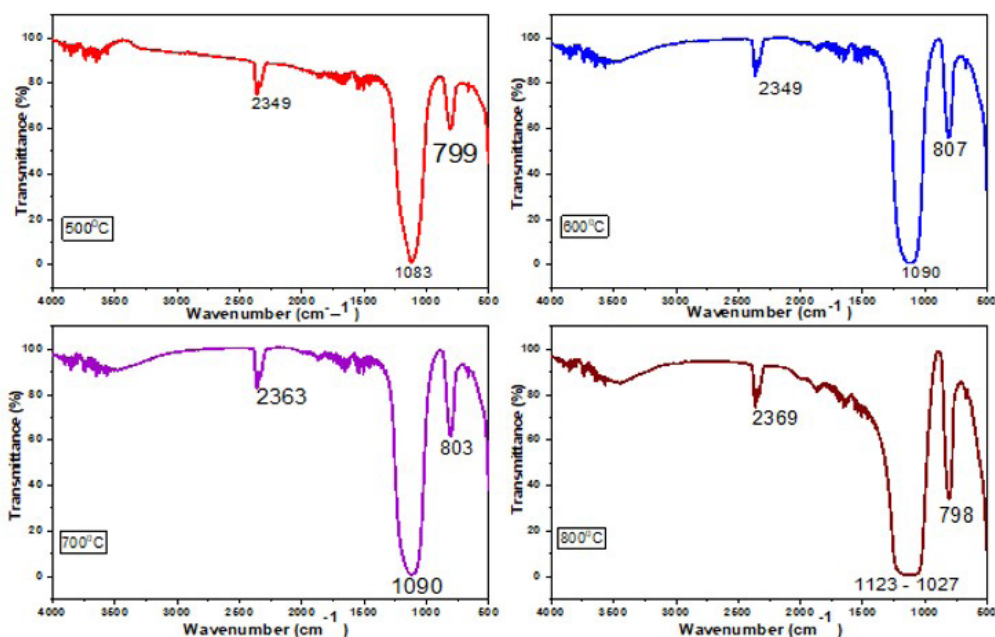


Figure 8: FTIR results of four heated fly ash samples

### Unheated samples

Figure 9 shows the FTIR result of the unheated fly ash. According to the analysis of this result, the wavenumber 2349 cm<sup>-1</sup> shows the appearance of O=C=O stretching vibrations, 1049 cm<sup>-1</sup> indicates the strong appearance of S=O stretching vibration of sulfoxide while 801 cm<sup>-1</sup> depicts the Si-O symmetric stretching vibration of the quartz. The frequency range for the strong absorption of sulfoxide compounds is 1070-1030.

It is observed that the unheated fly ash shows a strong appearance of O=C=O and S=O stretching. All five samples (both heated and unheated) show O=C=O bending with very strong stretching vibrations for the unheated sample and those heated at 500°C and 600°C while the third and fourth samples heated at 700°C and 800°C show a weak or medium appearance of O=C=O stretching. This suggests that the more the temperature the greater the chances of eliminating the carbon content in the fly ash. Samples 1, 2, and 3 heated at 500°C, 600°C, and 700°C respectively also show the appearance of Si-O-Si but not observed for the unheated and the heated samples at 800°C. The Si-O

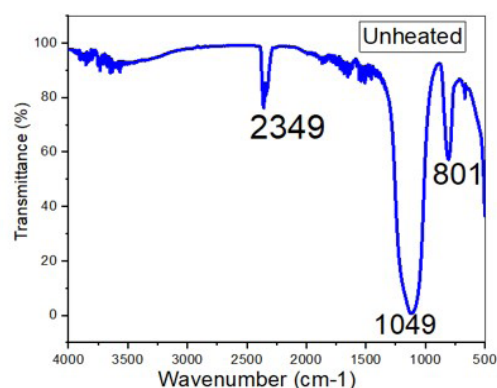


Figure 9: FTIR result of unheated fly ash sample

quartz appears in all five samples according to the FTIR result. Finally, it is observed from the FTIR result of this work that sulfoxide functional group (S=O) only appears in the unheated fly ash and is not seen in all the heated samples. This is an indication that sulfoxide in the raw fly ash easily disappears when subjected to a certain amount of heat.

**Table 1:** Wave numbers of different types of functional groups

Wavenumber (cm <sup>-1</sup> )	Compound	Functional	Reference
3454	Montmorillonite	OH group of absorbed water dust-stretching	(Summer, 1995)
2923	Organic carbon	C-H stretching vibration	(Hlavay, Jonas, Elek, & Inczedy, 1978)
1629	Organic matter	C=O carboxylate group	(Langford, Hodson, & Banwart, 2011; Matrajt <i>et al.</i> , 2004)
1384	Nitrate species	N-O stretching	(Smidt, Böhm, & Schwanninger, 2011)
1097	Quartz	Si-O-Si asymmetric stretching vibration	(Katara, Kabra, Sharma, Hada, & Rani, 2013)
794	Quartz	Si-O symmetric	(Coates, 1977)
463	Feldspar	Amorphous silica Si-O-Si band	(Karr, 2013)
2517	Calcite	Vibrational mode of carbonate	(Ramasamy, Rajkumar, & Ponnusamy, 2009)
1448	Calcite	C-O stretching for carbonate	(Ramasamy, Suresh, Meenakshisundaram, & Ponnusamy, 2011)
1032	Kaolinite	Si-O vibration of clay mineral	(Ramasamy, Rajkumar, & Ponnusamy, 2006)
873	Calcite	C-O bending for carbonate	(Dahlan, Mei, Kamaruddin, Mohamed, & Lee, 2008)
795	Quartz	Si-O symmetric	(Coates, 1977)
712	Calcite	Carbonate	(Adler & Kerr, 1963)
466	Feldspar	Si-O-Si bending	(Dahlan <i>et al.</i> , 2008)
1467	Calcite	C-O stretching for carbonate	(Ramasamy <i>et al.</i> , 2011)
2520	Calcite	Vibrational mode of carbonate	(Ramasamy <i>et al.</i> , 2006)
796	Quartz	Si-O symmetric	(Coates, 1977)
800, 802	Quartz	Si-O bending	(Ramasamy <i>et al.</i> , 2009)
1083, 1089		Si-O-Si stretching	(Ramasamy <i>et al.</i> , 2011)
1080, 1025		Si-O-Si stretching vibration	(Ramasamy <i>et al.</i> , 2011)
1020, 1090		Si-O-Si	(Ramasamy <i>et al.</i> , 2011)
910 - 830		Si-O stretching vibration	(Ramasamy <i>et al.</i> , 2006)
3550 - 3200	Alcohol	O-H	(Ramasamy <i>et al.</i> , 2006)
1685	Conjugated ketone	C=O stretching	(Ramasamy <i>et al.</i> , 2006)
1662-1626	Alkene	C=C	(Ramasamy <i>et al.</i> , 2006)
1205 - 1124	Tertiary alcohol	C-O stretching	(Smidt <i>et al.</i> , 2011)
1124 - 1087	Secondary alcohol	C-O stretching	(Smidt <i>et al.</i> , 2011)
1070 - 1030	Sulfoxide	S=O stretching	(Ramasamy <i>et al.</i> , 2006)
850 - 550	Halo compound	C-Cl stretching	(Ramasamy <i>et al.</i> , 2006)
840 - 790	Alkene	C=C	(Ramasamy <i>et al.</i> , 2006)
690 - 515	Halo compound	C-Br stretching	(Smidt <i>et al.</i> , 2011)
600 - 500	Halo compound	C-I stretching	(Smidt <i>et al.</i> , 2011)
1650 - 1556	Cyclic	Alkene	(Smidt <i>et al.</i> , 2011)
2400 - 2000	Carbon dioxide	O=C=O	(Smidt <i>et al.</i> , 2011)

### XRD Result

Material scientists and solid-state chemists use the powdered X-ray diffraction technique to determine the structure of a crystalline solid specimen under investigation. The diffraction pattern is formed by the interaction of the X-ray and atomic structure. Brag's law below is used to explain the direction of the scattered X-rays produced.

$$n\lambda = 2d\sin\theta$$

Where

$n$  = an integer

$\lambda$  = wavelength of the X-ray

$d$  = space between two layers of atoms

$\theta$  = angle between the incoming x-ray and the atom layer

The XRD results obtained from four heated and one unheated specimen of fly ash samples are explained in the figures below

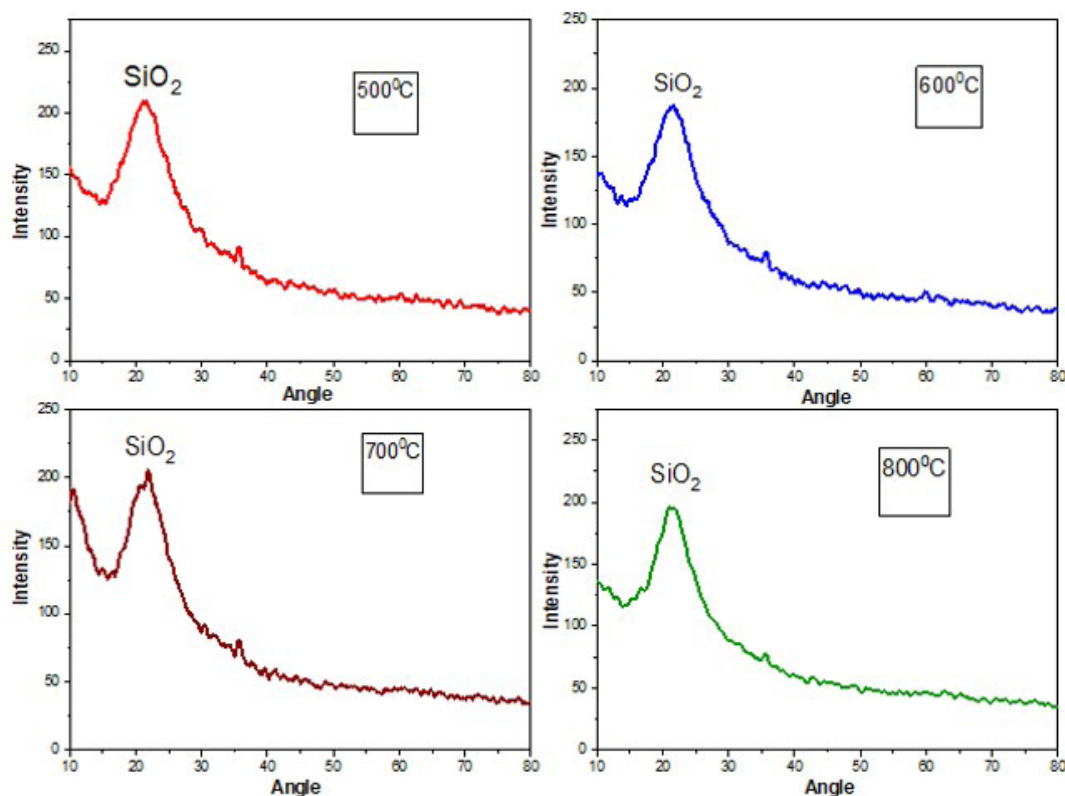


Figure 10: XRD result of heated fly ash

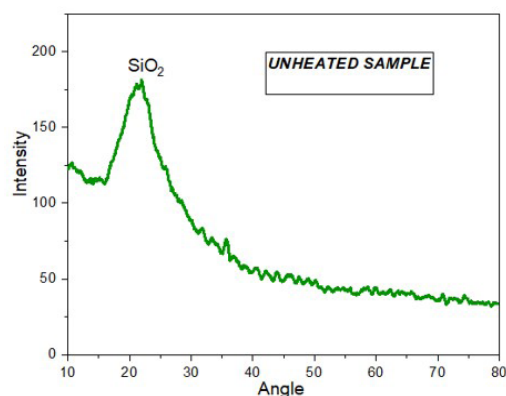


Figure 11: XRD result of unheated fly ash

The XRD result in figures 10 and 11 shows the presence of  $\text{SiO}_2$  in all the fly ash samples. This information is in line with the SEM/EDS and FTIR characterizations. The results and analysis of all the characterization in this work confirmed that the purified fly ash obtained from Xi'an Linyuan Silica Limited is pure silica.

## CONCLUSION

Critical analysis of the experimental results from the four characterization techniques shows that fly ash purely constitutes  $\text{SiO}_2$ , which is a significant constituent for the fabrication of refractory composites. According to the SEM/EDS results, the cenospheres discovered in the specimens are useful to refractory industrial engineers due to their low thermal conductivities and high heat resistance.

## Acknowledgments

This work was supported by the National Natural Science Foundation of China. Thanks, and appreciation to Wang Wei of the chemical engineering department, school of Water and Environment of Chang'an University for the adequate supervision and for providing the platform for the successful conduct of this work.

## REFERENCES

- Adler, Hans H, & Kerr, Paul F. (1963). Infrared spectra, symmetry and structure relations of some carbonate minerals. *American Mineralogist: Journal of Earth and Planetary Materials*, 48(7-8), 839-853.
- Adriano, DC, Page, AL, Elseewi, A A, Chang, AC, & Straughan, I. (1980). Utilization and disposal of fly ash and other coal residues in terrestrial ecosystems: a review. *Journal of Environmental quality*, 9(3), 333-344.
- Batra, Vidya S, Urbonaite, Sigita, & Svensson, Gunnar. (2008). Characterization of unburned carbon in bagasse fly ash. *Fuel*, 87(13-14), 2972-2976.
- Bird, Graeme A. (1994). Molecular gas dynamics and the direct simulation of gas flows. Molecular gas dynamics and the direct simulation of gas flows.
- Blissett, RS, & Rowson, NA. (2012). A review of the multi-component utilisation of coal fly ash. *Fuel*, 97, 1-23.
- Bourtsalas, Athanasios. (2015). Processing the problematic fine fraction of incinerator bottom ash into a raw material for manufacturing ceramics. Imperial College London.

- Bunge, Rainer. (2015). Recovery of metals from waste incinerator bottom ash. Removal, Treatment and Utilisation of Waste Incineration Bottom Ash; Holm, O., Thome-Kozmiensky, E., Eds, 63-143.
- Cheng, TW, & Chen, YS. (2003). On formation of CaO–Al<sub>2</sub>O<sub>3</sub>–SiO<sub>2</sub> glass–ceramics by vitrification of incinerator fly ash. *Chemosphere*, 51(9), 817-824.
- Coates, JP. (1977). The IR analysis of Quartz and Asbestos. Nelieth Offset Ltd., Chesham, England.
- Criado, María, Fernández-Jiménez, Ana, De La Torre, AG, Aranda, MAG, & Palomo, A. (2007). An XRD study of the effect of the SiO<sub>2</sub>/Na<sub>2</sub>O ratio on the alkali activation of fly ash. *Cement and concrete research*, 37(5), 671-679.
- Dahlan, IRVAN, Mei, GM, Kamaruddin, AZLINA HARUN, Mohamed, ABDUL RAHMAN, & Lee, KEAT TEONG. (2008). Removal of SO<sub>2</sub> and NO over rice husk ash (RHA)/CaO-supported metal oxides. *Journal of Engineering Science and Technology*, 3(2), 109-116.
- Erol, M, Küçükbayrak, S, & Ersoy-Mericboyu, A. (2008). Comparison of the properties of glass, glass–ceramic and ceramic materials produced from coal fly ash. *Journal of Hazardous Materials*, 153(1-2), 418-425.
- Fan, JR, Zha, XD, Sun, P, & Cen, KF. (2001). Simulation of ash deposit in a pulverized coal-fired boiler. *Fuel*, 80(5), 645-654.
- Fenelonov, Vladimir Borisovich, Mel'gunov, Maxim Sergeevich, & Parmon, Valentin N. (2010). The properties of cenospheres and the mechanism of their formation during high-temperature coal combustion at thermal power plans. *KONA Powder and Particle Journal*, 28, 189-208.
- Foday Jr, Edward Hingha, Bo, Bai, & Xu, Xiaohui. (2021). Removal of toxic heavy metals from contaminated aqueous solutions using seaweeds: A review. *Sustainability*, 13(21), 12311.
- Foday Jr, Edward Hingha, Ramli, Nurul As'shikin, Ismail, Hairu Nabilah, Malik, Nulhazwany Abdul, Basri, Hazlami Fikri, Aziz, Fatimah Syahirah Abdul, . . . Jumhat, Fairouz. (2017). Municipal solid waste characteristics in Taman Universiti, Skudai, Johore, Malaysia. *Journal of Advanced Research Design*, 38, 13-20.
- Gollakota, Anjani RK, Volli, Vikranth, & Shu, Chi-Min. (2019). Progressive utilisation prospects of coal fly ash: A review. *Science of the Total Environment*, 672, 951-989.
- Halmann, Martin M. (1995). Photodegradation of water pollutants: CRC press.
- Hlavay, Jozsef, Jonas, K, Elek, S, & Inczedy, J. (1978). Characterization of the particle size and the crystallinity of certain minerals by IR spectrophotometry and other instrumental methods—II. Investigations on quartz and feldspar. *Clays and Clay Minerals*, 26, 139-143.
- Hoomans, BPB, Kuipers, JAM, Briels, Willem J, & van Swaaij, Willibrordus Petrus Maria. (1996). Discrete particle simulation of bubble and slug formation in a two-dimensional gas-fluidised bed: a hard-sphere approach. *Chemical Engineering Science*, 51(1), 99-118.
- Joshi, Ramesh C, & Lohita, RP. (1997). Fly ash in concrete: production, properties and uses, 2, CRC Press.
- Karr, Clarence. (2013). Infrared and Raman spectroscopy of lunar and terrestrial minerals: Elsevier.
- Katara, S., Kabra, S., Sharma, A., Hada, R., & Rani, A. (2013). Surface modification of fly ash by thermal activation: a DR/FTIR study. *International Research Journal of Pure and Applied Chemistry*, 3(4), 299-307.
- Kim, Ann G. (2002). Physical and chemical characteristics of CCB. Paper presented at the Proceedings of Coal Combustion By-Products and Western Coal Mines: A Technical Interactive Forum. Allton, IL: US Department of the Interior, Office of Surface Mining.
- Langford, H., Hodson, A., & Banwart, S. (2011). Using FTIR spectroscopy to characterise the soil mineralogy and geochemistry of cryoconite from Aldegondabreen glacier, Svalbard. *Applied Geochemistry*, 26, S206-S209.
- Lee, FCC, & Lockwood, FC. (1999). Modelling ash deposition in pulverized coal-fired applications. *Progress in Energy and Combustion Science*, 25(2), 117-132.
- Lee, See Hoon, Lee, Tae Hee, Jeong, Sang Mun, & Lee, Jong Min. (2019). Economic analysis of a 600 mwe ultra supercritical circulating fluidized bed power plant based on coal tax and biomass co-combustion plans. *Renewable Energy*, 138, 121-127.
- Li, Gengda, Li, Shuiqing, Huang, Qian, & Yao, Qiang. (2015). Fine particulate formation and ash deposition during pulverized coal combustion of high-sodium lignite in a down-fired furnace. *Fuel*, 143, 430-437.
- Li, Lin, Wang, Shaobin, & Zhu, Zhonghua. (2006). Geopolymeric adsorbents from fly ash for dye removal from aqueous solution. *Journal of colloid and interface science*, 300(1), 52-59.
- Li, Shuiqing, Marshall, Jeffrey S, Liu, Guanqing, & Yao, Qiang. (2011). Adhesive particulate flow: The discrete-element method and its application in energy and environmental engineering. *Progress in Energy and Combustion Science*, 37(6), 633-668.
- Liu, Guanqing, Li, Shuiqing, & Yao, Qiang. (2011). A JKR-based dynamic model for the impact of micro-particle with a flat surface. *Powder Technology*, 207(1-3), 215-223.
- Maroto-Valer, MM, Taulbee, DN, & Hower, JC. (2001). Characterization of differing forms of unburned carbon present in fly ash separated by density gradient centrifugation. *Fuel*, 80(6), 795-800.
- Matrajt, G, Borg, J, Raynal, PI, Djouadi, Z, d'Hendecourt, L, Flynn, G, & Deboffe, D. (2004). FTIR and Raman analyses of the Tagish Lake meteorite: Relationship with the aliphatic hydrocarbons observed in the diffuse interstellar medium. *Astronomy & Astrophysics*, 416(3), 983-990.
- Miller, Bruce G. (2010). Clean coal engineering technology: Elsevier.
- Mishra, Barun, & Baliarsingh, Sandeep Kumar. (2008).

- Kinetics of iron ore reduction by coal and charcoal.
- Molina, A, & Poole, C. (2004). A comparative study using two methods to produce zeolites from fly ash. *Minerals Engineering*, 17(2), 167-173.
- Oves, Mohammad, Khan, Mohammad Saghir, Zaidi, Almas, & Ahmad, Ees. (2012). Soil contamination, nutritive value, and human health risk assessment of heavy metals: an overview: *Springer*.
- Pavlish, John H, Sondreal, Everett A, Mann, Michael D, Olson, Edwin S, Galbreath, Kevin C, Laudal, Dennis L, & Benson, Steven A. (2003). Status review of mercury control options for coal-fired power plants. *Fuel processing technology*, 82(2-3), 89-165.
- Pedersen, Kim Hougaard, Jensen, Anker Degn, Skjøth-Rasmussen, Martin Skov, & Dam-Johansen, Kim. (2008). A review of the interference of carbon containing fly ash with air entrainment in concrete. *Progress in Energy and Combustion Science*, 34(2), 135-154.
- Pundienė, Ina, Korjakins, Aleksandrs, Prancevičienė, Jolanta, & Kligys, Modestas. (2018). Effect of silicon carbide aggregate, prepared by different methods, on the properties of refractory concrete with cenospheres. *Ceramics International*, 44(13), 15944-15953.
- Rahman, A., Farrok, O., & Haque, M. M. (2022). Environmental impact of renewable energy source based electrical power plants: Solar, wind, hydroelectric, biomass, geothermal, tidal, ocean, and osmotic. *Renewable and Sustainable Energy Reviews*, 161, 112279.
- Ramasamy, V, Rajkumar, P, & Ponnusamy, V. (2006). FTIR spectroscopic analysis and mineralogical characterization of Vellar river sediments. *Bull. Pure Appl. Sci*, 25(1), 49-55.
- Ramasamy, V, Rajkumar, P, & Ponnusamy, V. (2009). Depth wise analysis of recently excavated Vellar river sediments through FTIR and XRD studies. *Indian journal of physics*, 83, 1295-1308.
- Ramasamy, V, Suresh, G, Meenakshisundaram, V, & Ponnusamy, V. (2011). Horizontal and vertical characterization of radionuclides and minerals in river sediments. *Applied Radiation and Isotopes*, 69(1), 184-195.
- Ratafia-Brown, Jay A. (1994). Overview of trace element partitioning in flames and furnaces of utility coal-fired boilers. *Fuel Processing Technology*, 39(1-3), 139-157.
- Richards, Galen H, Slater, Peter N, & Harb, John N. (1993). Simulation of ash deposit growth in a pulverized coal-fired pilot scale reactor. *Energy & Fuels*, 7(6), 774-781.
- Rios Reyes, Carlos A. (2008). Synthesis of zeolites from geological materials and industrial wastes for potential application in environmental problems.
- Schwarze, PE, Øvrevik, J, Låg, M, Refsnes, M, Nafstad, P, Hetland, RB, & Dybing, E. (2006). Particulate matter properties and health effects: consistency of epidemiological and toxicological studies. *Human & experimental toxicology*, 25(10), 559-579.
- Smidt, Ena, Böhm, Katharina, & Schwanninger, Manfred. (2011). The application of FT-IR spectroscopy in waste management. Fourier Transforms-New Analytical Approaches and FTIR Strategies. *Rijeka, Croatia: InTech*, 405-430.
- Summer, ME. (1995). Hand book of soil science, University of Georgia: Boca Raton Hondor press, New York.
- Tsuji, Y, Tanaka, Toshitsugu, & Yonemura, Shigeru. (1998). Cluster patterns in circulating fluidized beds predicted by numerical simulation (discrete particle model versus two-fluid model). *Powder Technology*, 95(3), 254-264.
- Valavanidis, Athanasios, Fiotakis, Konstantinos, & Vlachogianni, Thomais. (2008). Airborne particulate matter and human health: toxicological assessment and importance of size and composition of particles for oxidative damage and carcinogenic mechanisms. *Journal of Environmental Science and Health, Part C*, 26(4), 339-362.
- Vassilev, Stanislav V, Baxter, David, Andersen, Lars K, & Vassileva, Christina G. (2013). An overview of the composition and application of biomass ash. Part 1. Phase-mineral and chemical composition and classification. *Fuel*, 105, 40-76.
- Vassilev, Stanislav V, & Vassileva, Christina G. (1996). Mineralogy of combustion wastes from coal-fired power stations. *Fuel Processing Technology*, 47(3), 261-280.
- Waldmann, L, & Schmitt, KH. (1966). Thermophoresis and diffusiophoresis of aerosols *Aerosol science* (Vol. 137): Academic Press New York.
- Zeng, Xiongwei, Zheng, Shu, Zhou, Huaichun, Fang, Qingyan, & Lou, Chun. (2016). Char burnout characteristics of five coals below and above ash flow temperature: TG, SEM, and EDS analysis. *Applied Thermal Engineering*, 103, 1156-1163.